FWP.MT.GOV

THE **OUTSIDE** IS IN US ALL.

MONITORING UNGULATES IN NORTHERN FORESTS:

Camera-based estimates of abundance for mule deer, white-tailed deer, elk and moose in the Fisher River area

FINAL REPORT

May 10, 2022

MONTANA FISH, WILDLIFE & PARKS

UNIVERSITY OF MONTANA

MULE DEER FOUNDATION

RMEF

EXECUTIVE SUMMARY

In northwest Montana, monitoring of ungulate populations through traditional aerial survey methods is hampered by the low observability of animals through the forest canopy. Improved means for monitoring ungulates in this environment were recently identified as an important research priority within Montana Fish, Wildlife and Parks (MFWP). With this study, MFWP applied camera-traps for estimating abundance of multiple ungulate species to explore the potential of this technique to benefit long-term management.

We deployed 98 cameras at random locations across study area in the Fisher River drainage of hunting district 103, where winter range is shared by four cervid species. We monitored ungulates with time-lapse photos taken every 10 minutes and used space-to-event statistical procedures to estimate density and abundance of each species. We also analyzed a subset of data within an existing mule deer trend area to allow direct comparison of camera-based estimates for mule deer to spring aerial survey results from the years prior and following this study period. Estimates of density were achieved for each species, and from lowest to highest were 0.15 moose/km^2 , 0.31 elk/km^2, 2.69 mule deer/km^2, and 3.97 white-tailed deer/km^2. Random sampling allowed us to scale density estimates up to abundance estimates for the study area, yielding point estimates of 39 moose, 77 elk, 678 mule deer, and 1,004 white-tailed deer.

Within the Fisher River mule deer trend area, aerial surveys yielded spring counts of 360, 331, and 249, during two flights in 2019 and one flight in 2021, respectively. Space-to-event analysis of camera data within the trend area yielded an abundance estimate of 394 mule deer (95% CI [354–439]) for the winter of 2020. Assuming the underlying abundance of deer was constant during 2019–2021, this point estimate of abundance would suggest sightability estimates of 84–91% during the 2019 aerial survey flights and 63% during the 2021 survey. Such sightability would be within the range of estimates documented elsewhere in Montana, which suggests general agreement between techniques. Estimated mule deer density using only cameras within the trend area (d = 2.46 deer/km^2) was similar to that estimated using all cameras within the full winter range study area (d = 2.69 deer/km^2).

Effort to deploy cameras totaled 36 two-person crew-days in the field, with an average of 2.7–2.8 cameras deployed per day. Informal estimates of image processing time suggest roughly 49 person-days were required to view and classify images. Thus, considerable effort would be necessary to apply this technique more broadly across northwest Montana, but our results suggest multi-species monitoring across all four cervid species is possible.

Considerations for future applications include refining the field methods for defining and estimating camera viewsheds, addressing the potential effects of roads and trails on sampling and estimates, and evaluation of robust statistical estimates of variance when analyzing autocorrelated image data.

Suggested citation: DeCesare, N. J., C. White, T. Chilton-Radandt, J. Newby, P. Lukacs, and N. Anderson. 2022. Monitoring ungulates in northern forests: Camera-based estimates of abundance for mule deer, white-tailed deer, elk and moose in the Fisher River area. Final Report. Montana Fish, Wildlife and Parks, Helena, Montana.

INTRODUCTION

A foundational component of ungulate management in Montana is the annual monitoring of local population abundances and trends with aerial surveys (MFWP 2004). In the Northern Rockies ecoregion (Woods et al. 2002), monitoring of ungulate populations through traditional aerial survey methods is hampered by the low visibility of animals through the forest canopy. As a result, recent population trend estimates for deer, elk, and moose are unavailable for most hunting districts within northwest Montana's administrative Region 1. The inability to collect cost-effective and reliable data on the population size and trends of ungulates makes population management a challenge.

Further complicating such management is evidence of contemporary declines in some ungulate populations in this region. For example, in Region 1, mule deer (*Odocoileus hemionus*) hunter-harvest estimates have declined by 65% in just over a decade, from 2,320 to 822 deer harvested in 2005 versus 2017. Concurrently in 2017, 13.5 times as many white-tailed deer (*O. virginianus*) were harvested in the same region. Despite this imbalance, mule deer remain a species prized by the public, to the point that the first Region 1 mule deer permit area (where harvest of bucks is limited by permit) was created in 2018 in a subunit of HD 103 as the result of a proposal submitted by the public.

Wildlife managers in this portion of Montana are interested in investigating alternate means of obtaining reliable and cost-effective monitoring data for ungulates. Improved means for monitoring ungulates in this environment have recently been identified as an important long-term research priority within Montana Fish, Wildlife and Parks (MFWP). Fortunately, monitoring of ungulates in forested environments has also become a topic of active research elsewhere, with one particular tool showing promise. Trail cameras (or "camera traps") have provided wildlife managers and enthusiasts alike a means of monitoring rare or elusive species since the 1980s (Carbone et al. 2001). However, only recently has this tool been implemented as a new alternative for monitoring densities of more abundant populations of deer (Keever et al. 2017, Furnas et al. 2018) or elk (Moeller et al. 2018). Data developed from camera traps fail to meet the assumptions of some common statistical approaches (Parsons et al. 2017), yet alternative sampling and statistical methodologies are being developed for specific use with such methods and show promise for monitoring ungulates in northern forest environments (Moeller et al. 2018).

With this study, MFWP conducted its first application of camera-traps for estimating abundance to further explore rigorous monitoring practices for long-term management of ungulates. The specific project objectives were to:

1) deploy a grid of camera traps across a winter range shared by multiple ungulates in Region 1

2) estimate density and abundance of white-tailed deer, mule deer, elk (*Cervus canadensis*), and moose (*Alces alces*), using time-lapse photography paired with space-to-event modelling of animal density using the methods of Moeller et al. (2018), and

3) conduct mule deer aerial trend surveys for comparison with camera-based estimates.

STUDY AREA

Our research occurred in a portion of deer-elk hunting district (HD) 103 in the Fisher River drainage of northwest Montana. This general area was selected because it serves as an important winter range for all four of the sympatric cervid species in the region. The specific study area boundaries were drawn following an existing mule deer trend survey area to the east and the 6th order hydrologic unit (HUC) boundaries of the Fisher River Basin to the west. We estimated ungulate densities in this study area during 21 December 2019 – 20 March 2020.

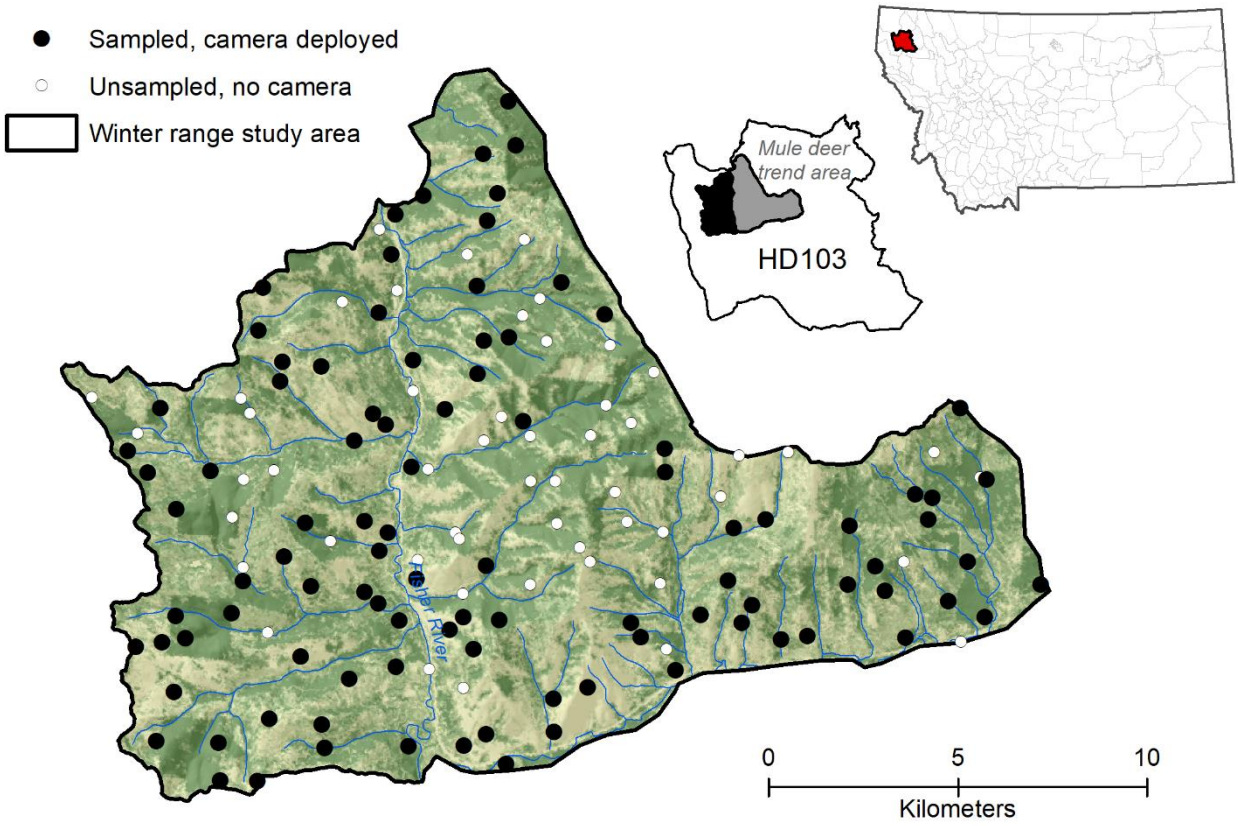

Figure 1. *Study area for camera-based ungulate monitoring during this study, including 150 random locations drawn to sample the area, only 98 of which were sampled with cameras, winter 2019–2020. Shown in the HD103 inset (in gray) is the subset of the study area designated as a mule deer trend area, where comparative aerial survey data were collected.*

METHODS

Data collection

We used the SDraw package in R (McDonald 2016) to draw a generalized random tessellation stratified (GRTS) sample of 150 locations within the study area (Figure 1). Then, during a 7-week period in November–December, 2019, field crews deployed cameras at 98 of those locations. We underestimated the time needed to deploy cameras in this manner, which included time to reach each

location, install cameras, and record viewshed measurements. Thus, the final sample of 98 cameras was less than our original target sample of 150, and some portions of the study area are under-represented (e.g., Cody Creek drainage) compared to what would be expected under a truly random sample of the entire study area. Density estimates for each species should be interpreted with this limitation in mind.

Cameras included a combination of Reconyx Hyperfire 2 (n = 63) and Hyperfire 1 (n = 19) models and Bushnell Core DS low glow models (n = 16). We adapted field protocols from colleagues at Idaho Fish and Game (S. Roberts, IDFG), and each camera deployment included the following steps.

1) Navigate to the pre-determined random location.
2) Identify the optimal camera and plot orientation within a 30-m area surrounding the location.
3) Deploy the camera on trees or t-posts, including additional brackets that facilitated aiming the camera parallel to the terrain slope.
4) Place snow stakes or reflective tape or flagging at 6 standardized locations (Figure 2).
5) Measure the viewshed by decomposing area in front of the camera into 6 circular sectors and recording the percent visibility to various distances, out to a maximum of 30 m, in each sector.

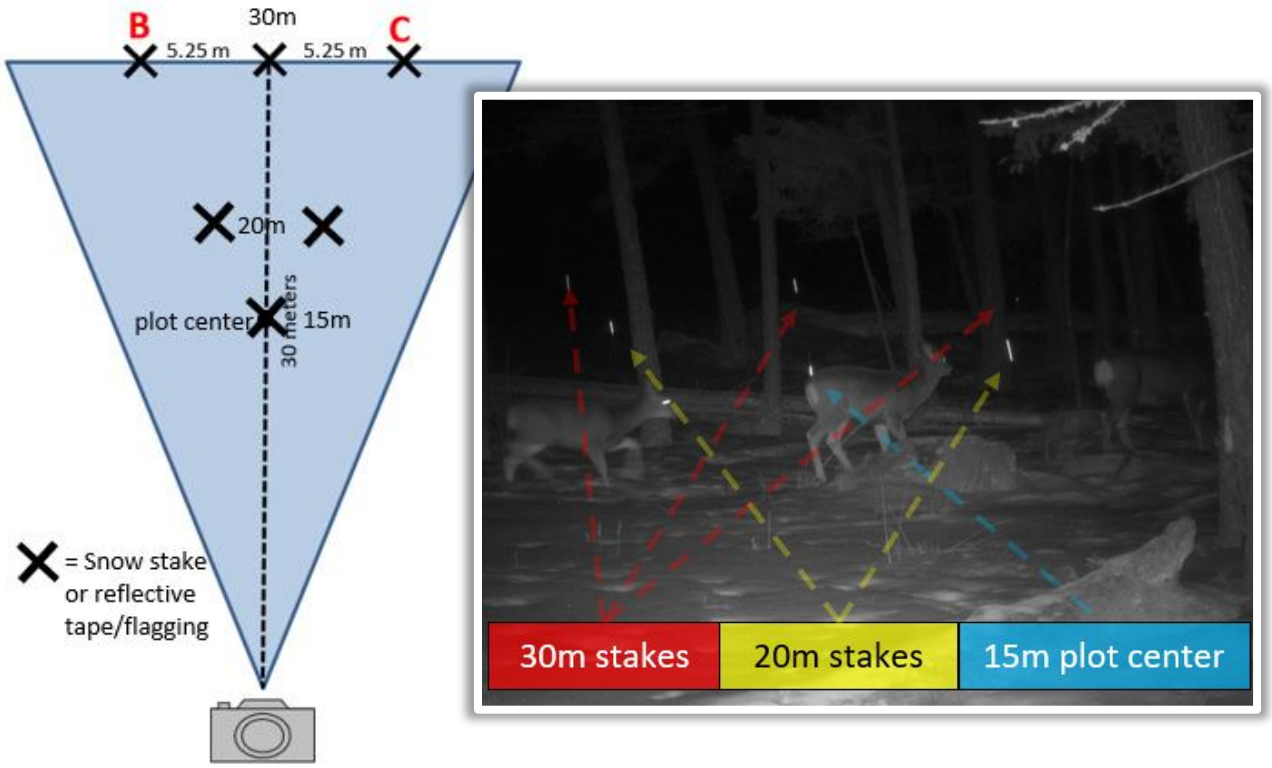

Figure 2. *An example camera viewshed, with reflective stakes placed at 3 distances (15m, 20m, and 30m) to document 3 viewshed radius distances for consideration during subsequent photo classification*.

Cameras were set to take time-lapse pictures every 10 minutes with motion-trigger pictures deactivated (Reconyx cameras) or to take pictures every 5 minutes with motion-trigger sensors covered with tape (Bushnell cameras). Cameras were left in the field for a 3-month winter season (December 21 – March 20), during which each camera could record a maximum of 13,104 pictures at 10-m intervals. We used reflective stakes and flagging to demarcate a maximum radius of 30-m for each camera viewshed. This 30-m distance was selected according to the flash distance of these camera models at night. Reflective

markers demarcating this radius allowed us to enforce the same viewshed radius and area when classifying images during both day and night. We also placed reflective markers at distances of 20 meters to demarcate an alternative, shorter, maximum radius in the event that camera flashes did not functionally reach far enough to sample a full 30-m viewshed. For these analyses, the 30-m maximum radius was used for all plots.

In the field, we divided plots into 6 sectors and used rangefinders to document the percent visibility to various distances within each sector. After using these measurements to account for reductions in visibility caused by heterogeneity in vegetation and topography, we calculated the area sampled by each viewshed unique to each camera deployment. It is important to account for these reductions in viewable area when measuring viewsheds to ensure unbiased animal density estimates that are specific to the viewable area sampled (Moeller et al. in review).

We retrieved cameras during 12 May – 23 July, 2020, and all images were classified manually within the software framework Timelapse (Greenberg et al. 2019), by technicians at the University of Montana during 1 June – September 30, 2021. Anecdotally, we estimated that images were classified at an average of roughly 1 per second, translating to 2.4 minutes of classification time per camera-day, or 3.6 hours per camera for the full 3-month season.

We classified images according to wildlife species, with the sole exception that in some cases we were unable to confidently assign images of deer (*Odocoileus* spp.) to one of the two resident species. Despite the lack of sufficient detail to discern species, these images were important samples of overall deer density and were important to include in analyses to avoid bias. We first included an additional "unknown deer" category, and assigned such cases accordingly. Upon completion of image classification, it became apparent from classified images that mule deer and white-tailed deer were reliably detected at different subsets of cameras (see Results). Thus, we subsequently assigned unknown deer to species according to whichever species was detected in majority at a given site.

Data analysis

We estimated density of each cervid species using space-to-event analysis of animal abundance in the spaceNtime package for program R (Moeller and Lukacs 2021). We constrained analyses to include only species detections that were within the measured viewsheds and excluded those beyond the 30-m plot boundary within which area was measured. We rounded all image times to the nearest 5-minute time stamp and subsampled all data to 10-minute time-lapse intervals to align data across camera models. We then conducted analyses with a 2-second sampling duration, and extrapolated density estimates across the entire 252.68 km^2 study area to estimate abundance. The naïve estimator produced variance and confidence interval estimates assuming each 10-minute sample was independent. Alternative resampling-based procedures for generating more robust estimates of variance are still under development and not available for use in this report.

RESULTS

Camera viewsheds varied substantially in the amount of area effectively viewable and thus sampled across sites (Figure 3). The average viewshed area was 255 m^2 (range 74–328), which represented a 23% decrease below the maximum of 328 m^2.

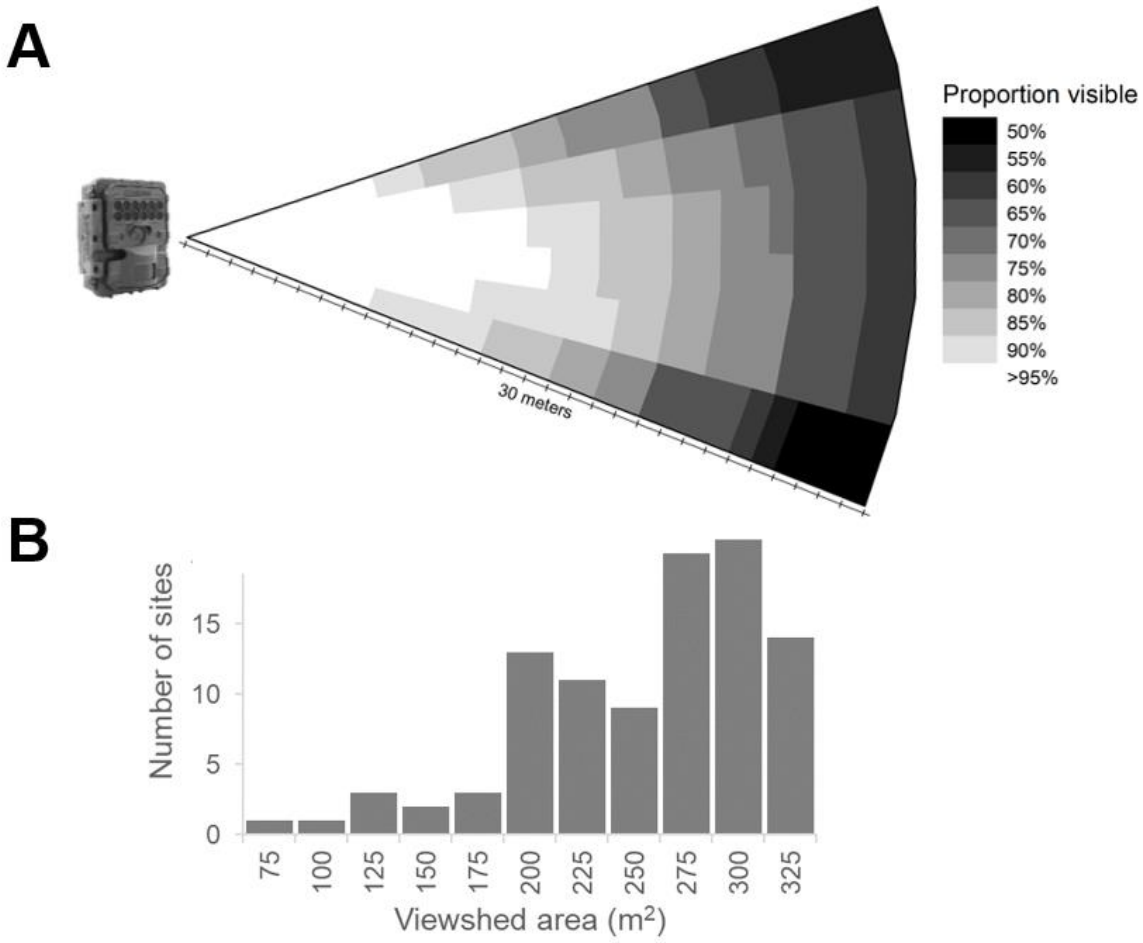

Figure 3. *Viewshed measurements at each camera site revealed A) a decrease in visibility further from the camera and along viewshed margins, and B) a relatively wide distribution in viewshed area per site.*

We analyzed data from 91 of 98 deployed cameras, after removing cameras with missing SD cards, issues with the timing of images (e.g., taking photos every 10 seconds instead of 10 minutes), premature battery failure, or other issues. There were substantial differences between camera make and model in the realized battery life in terms of days sampled and number of useable images, out of a maximum 92 days and 13,104 possible images (Table 1). Reconyx Hyperfire 2 cameras generally met expectations by averaging 89 out of 92 possible days and with 54 of 57 of included cameras lasting the for the full 92-day period. Contrarily, all Bushnell CoreDS cameras failed prior to completing 20 out of 92 scheduled days of monitoring.

Table 1. *Summary statistics for days of battery life and 10-minute timelapse images collected per camera by make and model of camera deployed in the study area, , excluding those not used in analyses, winter 2019–2020.*

Camera make/model	Number deployed	Days sampled		Images	
		Average	Range	Average	Range
Bushnell CoreDS LowGlow	16	17	(9–20)	2,227	(1184–2841)
Reconyx Hyperfire 1	19	71	(18–92)	10,109	(2491–13104)
Reconyx Hyperfire 2	63	89	(25–92)	12,589	(3499–13104)

Species detections

Images of white-tailed deer and mule deer were most common amongst species detections, with 51% and 46% of cameras recording at least one white-tailed deer or mule deer image (Table 2; Figure 4). Elk and moose were recorded less commonly, at 19% and 9% of cameras, respectively (Table 2; Figure 5). Detections of predator species were rare, including 8 mountain lion images (at 3 cameras), 0 wolf images, 2 bobcat images, and 1 coyote. No bear species were detected during the winter season, though 19 bear images (mostly black bear, ≥1 grizzly bear) were collected opportunistically at a minimum of 9 cameras during the spring until cameras were retrieved for processing.

Table 2. *Number of detections by species during the winter study period with 10-minute timelapse sampling (both total images and those specifically within the 30-m defined viewshed), as well as the percent of 91 cameras that included at least 1 image that was included in analyses, western Montana, 2019–2020.*

Species	Images included in analysis (within 30-m plot)	Total images (including beyond 30-m plot)	Percentage of cameras with ≥1 image
White-tailed deer	893	1361	51% (46 of 91)
Mule deer	651	918	46% (42 of 91)
Elk	74	144	19% (17 of 91)
Moose	37	42	9% (8 of 91)
Mountain lion	--*	8	3% (3 of 91)
Wolf	--*	0	0% (0 of 91)

*Formal analyses not conducted for predator species given few detections

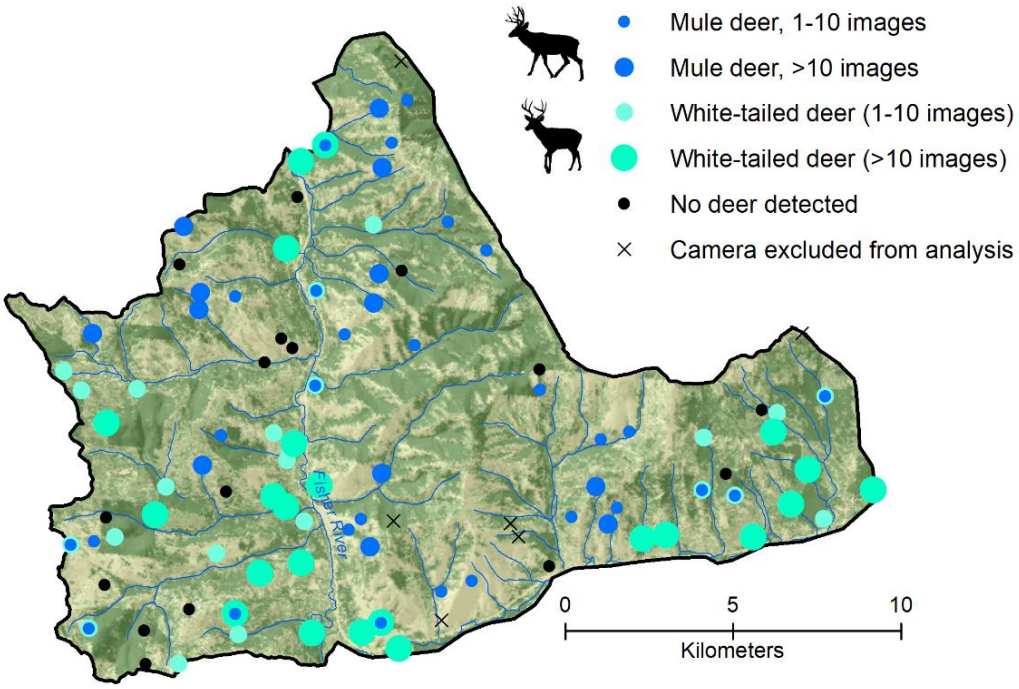

Figure 4. *Distribution of deer pictures collected with 10-minute time-lapse photography during the winter season, by species, excluding deer images initially categorized as unknown but later assigned to species.*

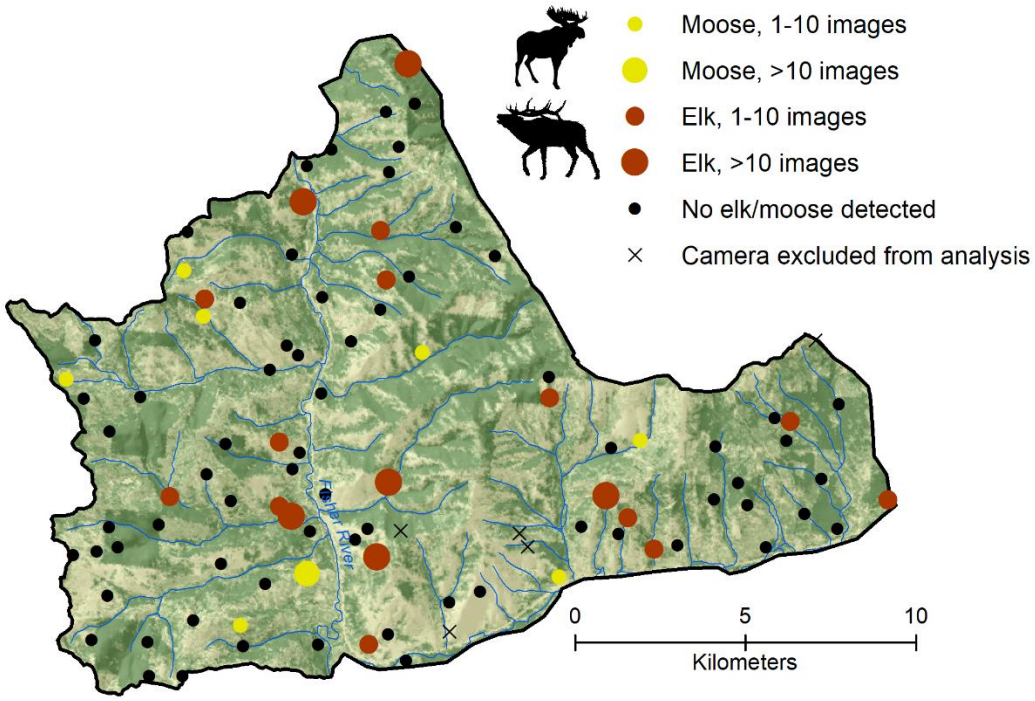

Figure 5. *Distribution of elk and moose pictures collected with 10-minute time-lapse photography during the winter season, by species.*

Abundance estimates

Estimates of density among cervids ranged from 0.15 moose/km^2 up to almost 4 white-tailed deer/km^2 (Table 3). Random sampling allowed us to scale density estimates up to abundance estimates for the study area, yielding point estimates of 39 moose, 77 elk, 678 mule deer, and 1,004 white-tailed deer within the study area (Table 3, Figure 6). Variance estimates from the STE estimator were relatively small, with the coefficient of variation decreasing in correspondence with increased density across species (Table 3). However, autocorrelation among 10-minute sequences of pictures likely does not meet assumptions of independent observations for using this estimator, and a robust method for properly estimating variance in this scenario is still under development (see Discussion).

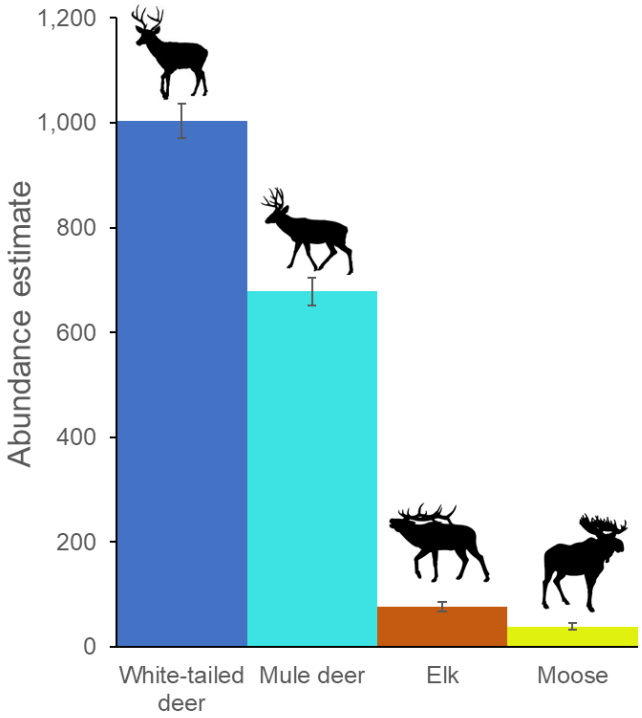

Figure 6. *Abundance estimates and 95% confidence intervals (assuming independence of observations) for 4 cervid species in the study area, winter 2019–2020.*

Table 3. *Space-to-event estimates of abundance, density, and associated coefficients of variation (CV) per species, for cervids in a winter range study area of HD103, 2019–2020.*

	Abundance			**Density**			**CV**
Species	N	SE	95% CI	N per km^2	SE	95% CI	
White-tailed deer	1,004	33.0	(942, 1071)	3.97	0.13	(3.73, 4.24)	3%
Mule deer	678	26.9	(628, 733)	2.69	0.11	(2.48, 2.90)	4%
Elk	77	9.0	(62, 97)	0.31	0.04	(0.24, 0.38)	12%
Moose	39	6.4	(28, 53)	0.15	0.03	(0.11, 0.21)	16%

Comparison to mule deer aerial survey data

We compared the mule deer distribution and abundance estimates from camera data to those collected via aerial surveys within a spring trend area used to monitor mule deer in HD103. Due to logistics of the COVID-19 pandemic, aerial surveys were not conducted during the spring immediately following our camera sampling in 2020. Thus, here we make comparisons to spring surveys conducted during years prior and following this study period, specifically April 2019 and April 2021. We first made visual comparisons of the distribution of mule deer detections between each method. We then re-estimated mule deer density and abundance with STE methods, but using data specific to the subset (n = 50) of cameras that were located within the trend area and included in analyses.

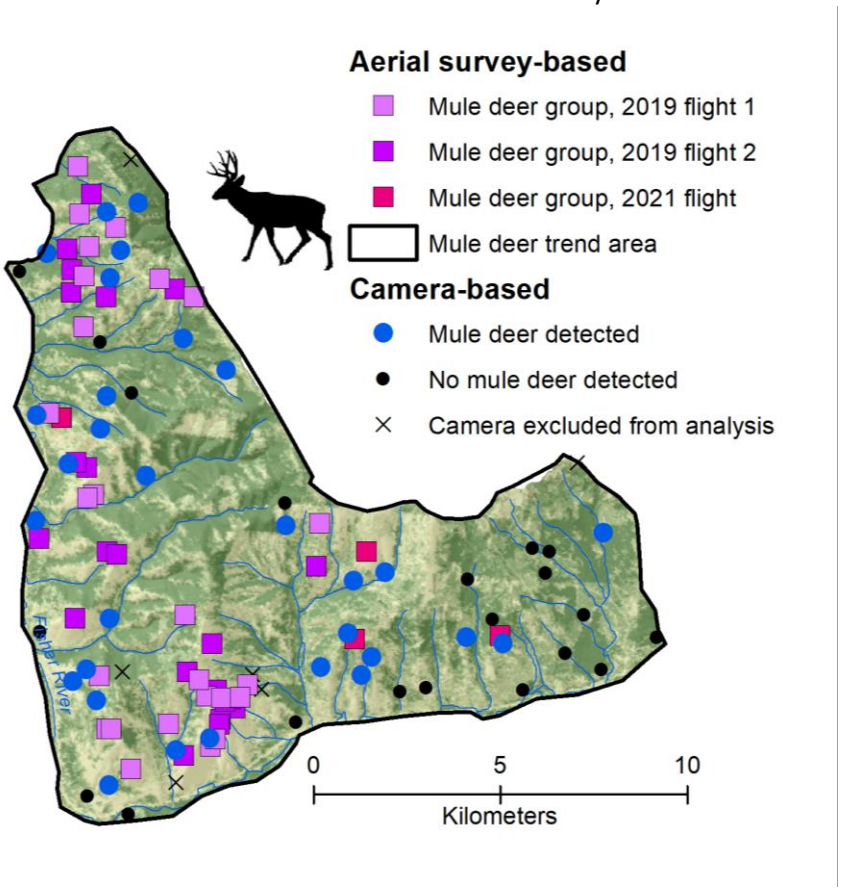

Figure 7. *Spatial location of mule deer detections from three spring aerial survey flights during 2019 and 2021 and from winter camera-based monitoring during 2020, specifically within the Fisher River mule deer survey trend area, which represented a subset of the total camera-based study area.*

Distributions of mule deer detections were generally well dispersed and similarly aligned between both aerial survey and camera methods (Figure 7). Aerial surveys showed somewhat higher concentration of deer on south-facing slopes in areas like Mount Sterling in the southwest corner of the trend area; these concentrations during spring green-up are known to occur following the winter season and partially drive the timing of aerial surveys.

Two aerial surveys were conducted during the spring of 2019 (April 29, April 30) and one survey was conducted during the spring of 2021 (April 17). Conditions during the 2019 surveys were classified as "good," with green-up underway and deer generally visible but difficult to classify due to light

conditions. Conditions during the 2021 survey were classified as "fair" because green-up was still in the early stages, the flight suffered from a late start (morning fog), and deer were more consistently found under forest cover. Minimum counts of mule deer were 360 and 331 during the 2019 surveys and 249 during the 2021 survey.

Space-to-event analysis of camera data within the trend area yielded an abundance estimate of 394 mule deer (95% CI [354–439]) for the winter of 2020. If we assume the underlying abundance of deer was constant across three winter and spring seasons of 2019–2021 surrounding the camera study, this point estimate of abundance would suggest sightability estimates of 84–91% during the 2019 aerial survey flights and 63% during the 2021 survey. Spring mule deer helicopter surveys elsewhere in Montana have averaged 57–74% sightability in various timbered study areas including the Bridger Mountains, Rocky Mountain Front, Missouri River Breaks, and Lower Stillwater (Mackie et al. 1998). Thus, the 2019 surveys labeled as "good" would correspond to above average sightability if aligned with camera estimates, but within the range of single-survey data achieved elsewhere, while the 2021 "fair" survey would correspond to expected average sightability when aligned with camera estimates.

Estimated mule deer density using only cameras within the trend area (d = 2.46 deer/km^2, 95% CI [2.21–2.75]) was similar to that estimated using all cameras within the full winter range study area (d = 2.69 deer/km^2, 95% CI [2.48–2.90]). Uncertainty surrounding the trend area density estimate (SE = 0.14, CV = 5.5%) was somewhat larger compared to that for the full study area and sample of cameras (SE = 0.11, 4.0%)

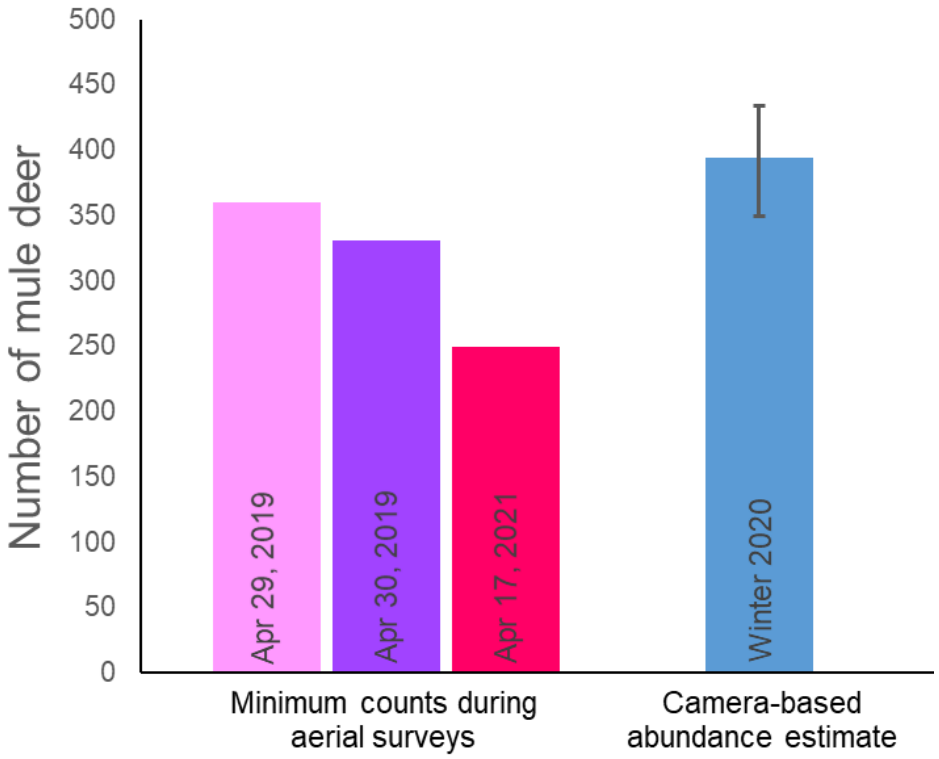

Figure 8. *Number of mule deer within the Fisher River trend area as measured by three helicopter-based spring aerial counts during 2019 and 2021 and an abundance estimate from STE-based analysis of camera data during winter 2020.*

DISCUSSION

Application of this technique to the ungulate winter range in the Fisher River yielded adequate data for estimation of ungulate densities. Furthermore, those estimates were reasonably matched to biologists' expectations in the area and with aerial survey data for mule deer. While these comparisons do not represent rigorous validation or calibration with independent data for all species, they do suggest a practical utility of such data for management.

A consideration for putting such an approach into practice is the workload and time required. Deploying 98 cameras in this study area required 36 field days for a two-person crew. In this study the work was divided across 3 crews, who worked 11, 12, and 13 days each. Crews were very similar in their efficiency in deploying cameras, averaging 2.7, 2.7, and 2.8 cameras deployed per day and ranging from 1 to 5 (Figure 9). Expanding the sampling frame to an entire HD would likely decrease this efficiency by increasing the distance between randomly sampled locations. Retrieving cameras was more efficient, ranging from 1–9 cameras per day and requiring only a single person in many cases.

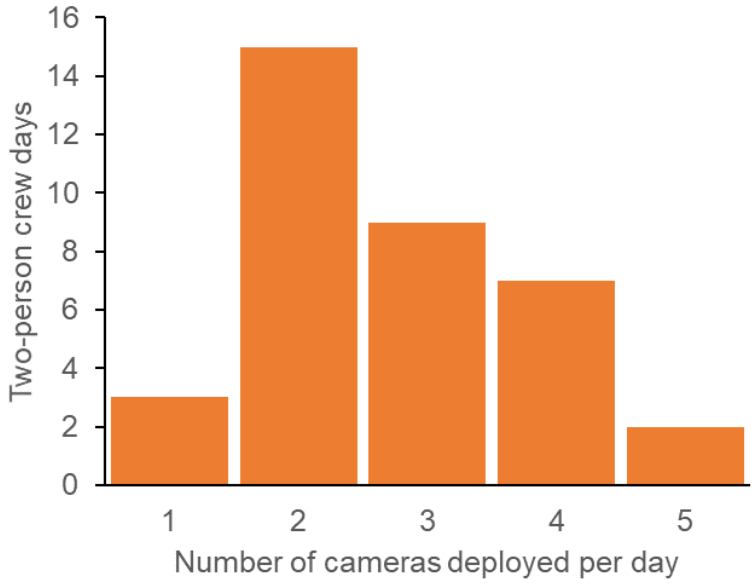

Figure 9. *Histogram of the frequency of two-person crew workdays according to how many cameras were deployed by a single crew. There were three crews that each averaged 2.7–2.8 cameras deployed per day, November–December, 2019.*

While field work represented a significant amount of time and effort, processing images was the biggest hurdle towards completing this project. The onset of the COVID-19 pandemic caused delays in recruiting technicians for image processing, a process which lasted 12 months in total. Informal estimates of the time required to classify photos (1 image/second) suggest a full 3-month data set of >13,000 images for a single camera would take about 4 hours. Translating this to 8-hour work-days yields 49 person-days for a data set of 98 cameras. Thus, improvements to the 12-month processing time are possibl, but the time and effort required for image processing remain significant and will delay survey results after camera retrieval. Automated analysis of images using artificial intelligence is a burgeoning area of research, and could eventually offer an alternative to the people and time required for extracting data from images (Norouzzadeh et al. 2018). Both free and fee-for-service alternatives are currently in development but have not been fully vetted to meet this need at MFWP.

Space-to-event analyses assume independence among sampling intervals, or in other words, that animals redistribute themselves in between images. With 10-minute time-lapse images, this assumption is clearly not met. As evidence of such, a non-trivial proportion of animal detections included animals bedded down in front of cameras for multiple images in succession. Bootstrapping, or randomly resampling cameras with replacement and estimating density across resamples, may yield a corrected variance estimate that accounts for within-camera autocorrelation (Ausband et al. 2021). However, our initial trials of this approach suggested a negative bias of resampling with replacement on time-to-event analyses induced by redundant detections within the same time interval when a given camera is resampled more than once. Other approaches such as jackknife resampling or resampling without replacement according to subsets of time or space may offer alternatives to this approach, but have not been fully vetted.

Another consideration for future applications is the measurement of viewshed areas and inclusion of field markers that delineate various distances within viewsheds. This aspect of camera-based sampling has recently been reviewed by Moeller et al. (in review) and has implications for density estimates. In practice, it is difficult to quantify the proportion of viewsheds that are obscured because of the variable nature of detectability across species, sexes, postures, spatial orientation, and the like. Our recommendation for future work would be to simplify this process by dividing the viewshed into a higher number of conical sectors and marking a maximum distance of consideration in each sector within which detectability can be assumed to be 100%. This may result in the loss of some detections in areas that are partially obscured, but should yield robust results (Moeller et al. in review).

Lastly, there is a need for additional research into the effects of spatial heterogeneity in animal space use and movement on density estimates founded upon random sampling. With an infinite number of cameras, such heterogeneity would be adequately captured by a random sample and yield unbiased estimates. However, at lower sample sizes or higher degrees of concentrated movements (such animals showing a strong preference for movement on roads and trails), it is conceptually possible a random sample might underestimate density if such rare but important features are not adequately represented. In our study, this concern may have been exacerbated by decisions to censor (i.e., not deploy cameras at) random cameras that happened to fall on openly accessible roads, due to concerns over risk of theft. On the other hand, specifically targeting roads and trails for sampling is known to cause the opposite problem of biasing density estimates high (Kolowski and Forrester 2017). More work is needed to address the constraints of, or alternatives to, random sampling in such an environment.

ACKNOWLEDGMENTS

Dedicated funding for this study was provided by the Montana Chapter of the Mule Deer Foundation and the Rocky Mountain Elk Foundation Project Advisory Committee program in Montana. Support was also provided by Montana Fish, Wildlife and Parks and the University of Montana. We thank Christian Meny, Kathleen Petersen, and Justine Vallieres who put forth great effort to deploy cameras. We also thank many people who assisted with collecting cameras at the completion of the study period, including Lee Anderson, Marco DeCesare, Franz Ingelfinger, Sawyer Johnson, Ethan Lula, Chris Neu, Bruce Sterling, and Doug Whitman. Thanks also to Caryn Dearing, Justin Gude, and others at FWP for support of project logistics. Jon Horne, Mark Hurley, Josh Nowak, and Shane Roberts provided crucial guidance regarding sampling design and field methodologies. We also thank Christian Dupree and others at University of Montana for their dedication and time spent classifying images. We thank

Weyerhaeuser, Stimson Lumber, Montana DNRC, and the Kootenai National Forest for permissions to access and deploy cameras on lands within the study area.

LITERATURE CITED

Ausband, D. E., P. M. Lukacs, M. Hurley, S. Roberts, K. Strickfaden, and A. K. Moeller. 2022. Estimating wolf abundance from cameras. Ecosphere 13:e3933.

Carbone, C., et al. 2001. The use of photographic rates to estimate densities of tigers and other cryptic mammals. Animal Conservation 4:75–79.

Furnas, B. J., et al. 2018. Integrated modeling to estimate population size and composition of mule deer. Journal of Wildlife Management 82:1429–1441.

Keever, A. C., et al. 2017. Efficacy of N-mixture models for surveying and monitoring white-tailed deer populations. Mammal Research 62:413–422.

Kolowski, J. M., and T. D. Forrester. 2017. Camera trap placement and the potential for bias due to trails and other features. PLoS One 12:e0186679.

McDonald, T. 2016. Package 'SDraw': spatially balanced sample draws for spatial objects.

MFWP (Montana Fish, Wildlife, and Parks). 2004. Montana statewide elk management plan. Montana Fish, Wildlife and Parks, Helena.

Moeller, A. K., and P. M. Lukacs. 2021. spaceNtime: an R package for estimating abundance of unmarked animals using camera-trap photographs. Mammalian Biology: s42991-021-00181-8

Moeller, A. K., P. M. Lukacs, and J. S. Horne. 2018. Three novel methods to estimate abundance of unmarked animals using remote cameras. Ecosphere 9(8):e02331.

Moeller, A. K., S. J. Waller, N. J. DeCesare, M. C. Chitwood, and P. M. Lukacs. In review. Best practices to account for capture probability and viewable area in camera-based abundance estimation. Remote Sensing in Ecology and Conservation.

Norouzzadeh, M. S., A. Nguyen, M. Kosmala, A. Swanson, M. S. Palmer, C. Packer, and J. Clune. 2018. Automatically identifying, counting, and describing wild animals in camera-trap images with deep learning. Proceedings of the National Academy of Sciences 115:E5716–E5725.

Parsons, A. W., et al. 2017. Do occupancy or detection rates from camera tarps reflect deer density? Journal of Mammalogy 98:1547–1557.

Woods, A.J., Omernik, J.M., Nesser, J.A., Shelden, J., Comstock, J.A., and S. H. Azevedo. 2002. Ecoregions of Montana, 2nd ed.